Soft Matter

Heterogeneous distribution of kinesin-streptavidin complexes revealed by Mass Photometry

Journal:	*Soft Matter*
Manuscript ID	SM-COM-12-2023-001702.R2
Article Type:	Communication
Date Submitted by the Author:	19-May-2024
Complete List of Authors:	Xu, Jing; University of California Merced, Department of Physics Brown, Nathaniel; University of California Merced, Department of Quantitative and Systems Biology Seol, Yeonee; NIH, Laboratory of Single Molecule Biophysics, National Heart, Lung and Blood Institute Neuman, Keir; NIH, Laboratory of Single Molecule Biophysics, National Heart, Lung and Blood Institute

COMMUNICATION

Heterogeneous distribution of kinesin-streptavidin complexes revealed by Mass Photometry

Received 00th January 20xx,
Accepted 00th January 20xx

DOI: 10.1039/x0xx00000x

Jing Xu,*[a] Nathaniel J. S. Brown,[b] Yeonee Seol[c] and Keir C. Neuman[c]

Kinesin-streptavidin complexes are widely used in microtubule-based active-matter studies. The stoichiometry of the complexes is empirically tuned but experimentally challenging to determine. Here, mass photometry measurements reveal heterogenous distributions of kinesin-streptavidin complexes. Our binding model indicates that heterogeneity arises from both the kinesin-streptavidin mixing ratio and the kinesin-biotinylation efficiency.

Kinesin-streptavidin complexes are widely used to drive filament-filament sliding in microtubule-based active matter studies[1-8]. The complexes are typically formed via incubating biotinylated kinesin dimers with streptavidin tetramers. Each kinesin dimer contains up to two biotins[9-11], and each streptavidin tetramer can bind up to four biotins. The resulting complexes are generally assumed to contain a homogeneous population of two kinesin dimers and one streptavidin tetramer, corresponding to a 2:1 complex stoichiometry. This assumption, however, has not been experimentally verified. Instead, an early study employing analytical gel filtration suggested up to 8 kinesin dimers per complex[2], and recent work employing dynamic light scattering estimated a stoichiometry of four kinesin dimers per streptavidin tetramer[8]. Furthermore, the assumption of a homogeneous population of 2:1 complex stoichiometry is challenged by experimental findings that the macroscopic dynamics of the active matter system depend sensitively on the mixing ratio of kinesin dimers to streptavidin tetramers[1, 4]. Specifically, under otherwise identical conditions, Henkin et al. reported a ~2.6-fold linear decrease in the characteristic length scale of the active matter system as the mixing ratio increased by ~3.8-fold from ~0.9 to 3.4 kinesin dimers per streptavidin tetramer[4]. Moreover, the characteristic length scale of the system decreased as the concentration of kinesin-streptavidin complexes increased[4], or the concentration of ATP in the assay decreased[4]. The common effect of increasing concentrations of kinesin-streptavidin complexes and decreasing concentrations of ATP (which reduces kinesin's off-rate from the microtubule[12]) is an increase in the number of kinesins simultaneously bound to microtubules. These empirical findings therefore indicate an inverse correlation between the number of kinesins simultaneously bound to microtubules and the characteristic length scale of the active matter system. This effect is distinct from experiments in which an increase in the microtubule crosslinker PRC1 increased the characteristic length scale[13]. It remains to be determined how these experimental findings may be understood within the framework of established theoretical models[14, 15]. In the current study, we hypothesized that the decrease in the characteristic length scale with increasing mixing ratios[4] reflects an increase in the relative abundance of kinesin-streptavidin complexes with stoichiometries exceeding 2:1, containing more kinesins that can simultaneously bind microtubules.

Quantitative characterization of kinesin-streptavidin complex stoichiometry is experimentally challenging. For example, the relatively high concentrations of proteins required for analytical gel filtration or ultracentrifugation can induce non-specific aggregates that are otherwise not present at the sub-μM concentrations employed in active-matter work. Although dynamic light scattering can detect particle sizes at dilute concentrations, the resulting size distribution is strongly sensitive to assumptions of protein shape and is further complicated by the strong dependence of scattering intensity on the individual masses of scattering particles[16, 17]. Native polyacrylamide gel electrophoresis (native PAGE), another important technique for characterizing protein complexes in the native form, is sensitive to the shape and net charge, as well as the molecular mass, of the protein[18]. Finally, fluorescence-

[a] *Department of Physics, University of California, Merced, CA 95343, USA. Email: jxu8@ucmerced.edu*
[b] *Department of Quantitative and Systems Biology, University of California, Merced, CA 95343, USA*
[c] *Laboratory of Single Molecule Biophysics, National Heart, Lung and Blood Institute, NIH, Bethesda, MD 20892, USA*
† Electronic Supplementary Information (ESI) available: [details of any supplementary information available should be included here]. See DOI: 10.1039/x0xx00000x

based methods, such as stepwise photobleaching, are complicated by incomplete fluorescence-labelling of proteins[19].

Mass photometry is a recently-developed, label-free, technique for determining the mass and the relative abundance of proteins and protein complexes in dilute solutions[20]. Similar to dynamic light scattering, mass photometry is a light scattering-based technique[21-24]. Distinct from dynamic light scattering that employs the interference between light scattered from distinct particles in solution, mass photometry utilizes the interference between light reflected by the sample surface and light scattered by individual particles on the same surface (Fig. 1a). As the result, for each particle that binds the sample surface from solution, mass photometry returns a concentric ring pattern characteristic of the interference between a plane wave (reflected by the fixed sample surface) and a spherical wave (scattered by the bound particle) (Fig. 1b). The intensity of the plane wave (reflected by the fixed sample surface) is kept constant, yielding a peak interference intensity that is proportional to the polarizability of the bound particle. For simple dielectric materials, the polarizability of a particle scales linearly with the volume and thus the mass of the particle. This linearity between interference intensity and the mass of the particle is demonstrated in mass photometry over a broad mass range of ~50-5000 kDa[25]. Heterogeneity in interference intensities reveal multiple mass species in solution (Fig. 1b, bottom panel), and molecular counting of different mass species yields the relative abundance of individual mass species in solution.

In the current study, we carried out mass photometry measurements using a commercial OneMP instrument (Refeyn, UK). We verified that the interference intensity reported by the OneMP instrument scales linearly for masses up to 1048 kDa (Fig. S1, ESI†); this broad linear range is appropriate for determining the molecular mass and thus the stoichiometry of kinesin-streptavidin complexes in the current study. We employed the resulting mass versus interference intensity calibration to convert individual interference intensities from mass photometry images (for example, Fig. 1b) into individual molecular masses.

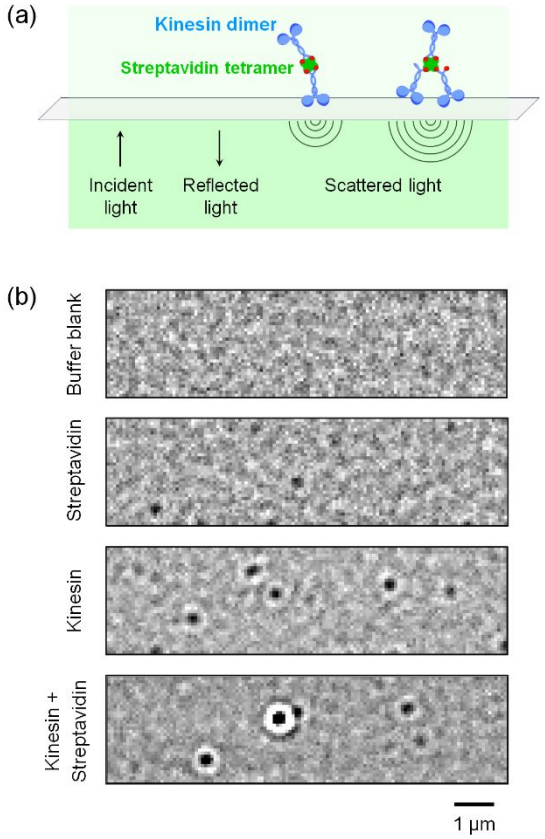

Fig. 1 (a) Illustration of mass photometry experiments, in which scattered light from protein complexes on the sample surface interferes with reflected light from the same surface. Illustration is not to scale. (b) Representative mass photometry images of protein-free buffer (top) and protein solutions (bottom three panels). Scale bar, 1 μm. Interference intensity of each spot scales linearly with molecular mass; heterogeneity in spot intensities reveal multiple species of protein complexes in solution (bottom).

We prepared kinesin-streptavidin complexes by incubating solution mixtures of kinesin dimers and streptavidin tetramers on ice for 30 min following standard protocols[1, 6, 7]. We varied the kinesin-streptavidin mixing ratio between 0.4-3.6 kinesin dimers per streptavidin tetramer, encompassing the range of mixing ratios previously identified to impact the characteristic length scale in active matter[4]. Note that this prior work[4] specified the mixing ratios but not the associated protein concentrations. Based on the common range of kinesin concentrations in literature[1, 6, 7], and to reduce the likelihood of artifactual protein aggregation that can occur at high kinesin concentrations[7], we limited the concentration of kinesin dimers to ≲2-3 μM for the majority of the measurements in the current study. Accordingly, we employed a constant concentration of streptavidin tetramers (0.6 μM) and varied the concentration of kinesin dimers to achieve the indicated mixing ratio. Given the relatively fast binding rate of biotin to streptavidin (~3-75 $\mu M^{-1}s^{-1}$)[26, 27] and the exceedingly slow dissociation rate (~10^{-6} s^{-1})[28, 29], we expect kinesin-streptavidin binding to be complete and stable within the 30 min incubation and subsequent measurement time. We estimated the concentrations of the isolated proteins via absorption measurements at 280 nm, and

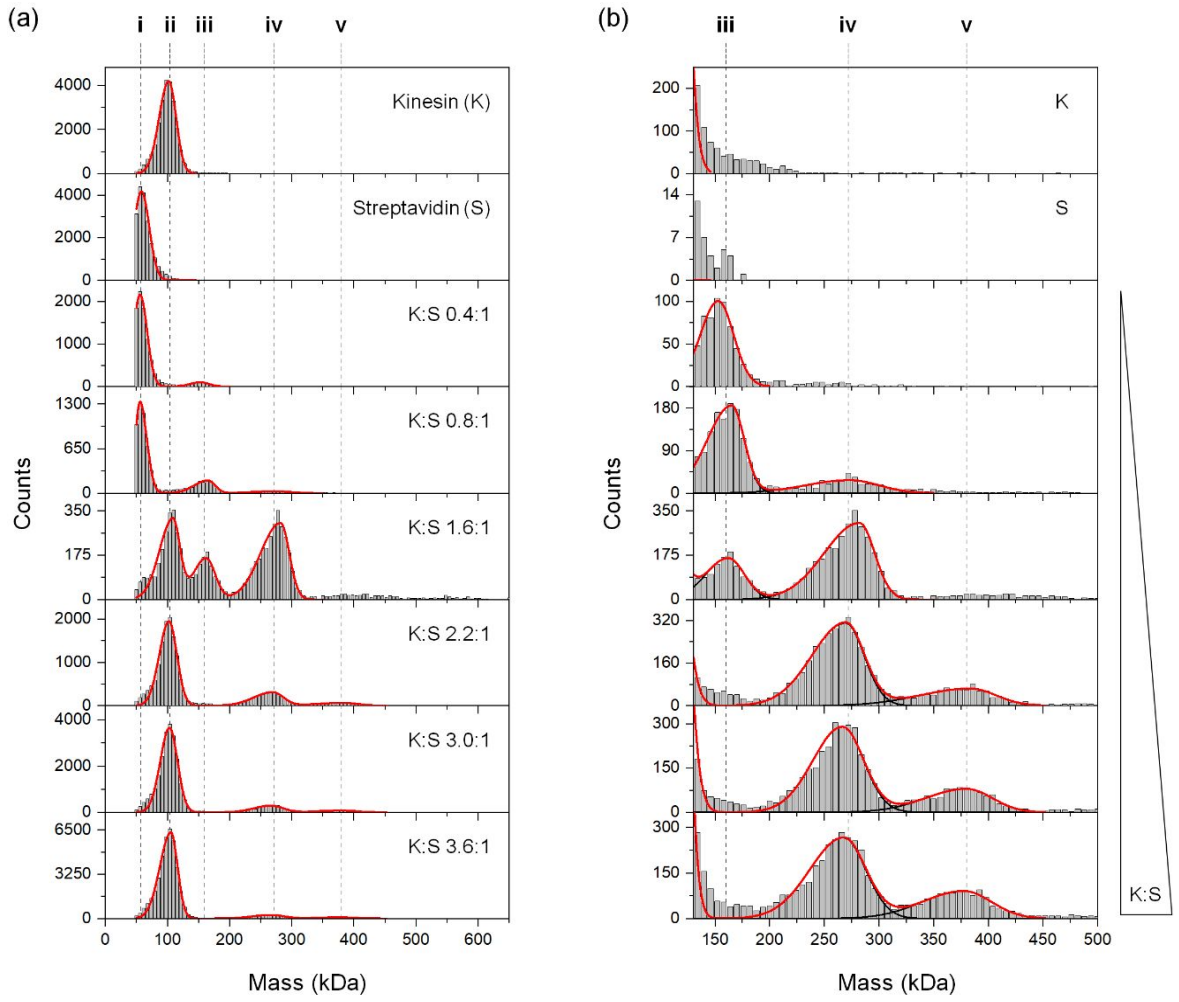

Fig. 2 (a) Distributions of molecular masses revealed by mass photometry. Solutions contain kinesin (K), streptavidin (S), and their mixtures (K:S). K:S indicates the molar ratio of kinesin dimers to streptavidin tetramers in each mixture ("mixing ratio"). The concentration of streptavidin in each mixture was kept constant at 0.6 μM. Each distribution represents data pooled from 12-22 independent measurements. Dashed lines indicate molecular masses of identified major species; red lines indicate best fits of mass distributions to a bi-Gaussian mixture model (Materials and Methods, ESI†). To ensure fitting accuracy, only mass species with pronounced peak profile (>40 in peak height, or >400 counts) were included in the fit. (b) Expanded view of mass species iii-v. Red lines and dashed lines are as described in (a). Black lines indicate contributions of individual species to the fit.

we determined the mixing ratio for each preparation of kinesin-streptavidin complexes via quantitative densitometry of proteins stained with Coomassie blue (Fig. S2, ESI†).

We diluted each preparation of kinesin-streptavidin complexes to 20 nM total protein concentration, within the mass-photometry working concentration range (0.1-100 nM[25, 30]). For each fresh dilution of protein solutions, we imaged the individual binding events for a fixed measurement duration of 1 min. This measurement duration, typical in mass photometry experiments, is short compared to the exceedingly slow dissociation rate of biotin-streptavidin binding (~10^{-6} s^{-1})[28, 29]. Together, the short measurement duration and the dilute protein concentration preserve complex integrity while avoiding protein aggregation. Solutions containing isolated proteins were used as controls.

We performed 12-22 independent mass photometry measurements for each preparation of kinesin-streptavidin complexes or isolated protein controls. We detected no substantial variations among independent measurements using the same sample (Fig. S3a, ESI†) or using different preparations of the same kinesin-streptavidin mixture (Fig. S3b, ESI†). We pooled these independent measurements to determine the distribution of mass species in each protein solution (Fig. 2). We fitted the resulting mass distributions to a bi-Gaussian mixture model (red lines, Fig. 2) to first determine the molecular masses of the major species (dashed lines i-v, Fig. 2). To ensure fitting accuracy, only mass species with pronounced peak profiles (>40 in peak height, or >400 counts total) were included in the fit (red lines, Fig. 2).

We detected single mass species in control solutions of isolated proteins (top two panels, Fig. 2a). The molecular masses of each species are in good agreement with the theoretical masses of the streptavidin tetramer and the kinesin dimer (i-ii, Fig. 3), as well as a prior mass photometry

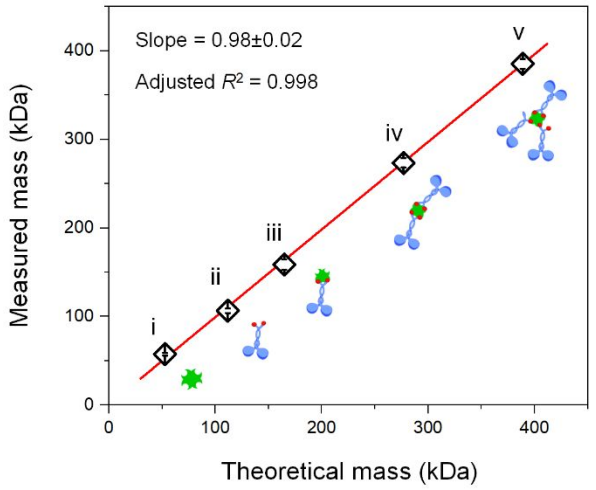

Fig. 3 Theoretical *vs*. measured masses for major species revealed by mass photometry. Red line indicates best linear fit with zero intercept. slope = 0.98±0.02 and adjusted R^2 = 0.998. Cartoons illustrate streptavidin (i), kinesin (ii), and kinesin-streptavidin complexes with 1:1, 2:1, and 3:1 stoichiometry (iii, iv, and v, respectively). Measured masses were determined via the best-fits in Fig. 2 (dash lines i-v). Error bars indicate standard deviation. N = 4-12.

measurement of the streptavidin tetramer (57.2 ± 1.5 kDa in the current study *vs*. 55.7 ± 1.1 kDa previously[20]). These results validate the accuracy of mass photometry and demonstrate no significant protein aggregates in either protein solution.

In contrast, we detected multiple mass species in solutions containing both kinesin and streptavidin (bottom six panels, Figs. 2a and 2b). In addition to the two isolated proteins, mass photometry revealed three larger species (iii-v, Figs. 2a and 2b). The molecular masses of these larger species are highly correlated with theoretical molecular masses for complexes containing up to three kinesin dimers and one streptavidin tetramer (iii-v, Fig. 3). Note that the correspondence between mass and complex stoichiometry is not necessarily unique, given that the molecular mass of the kinesin dimer is approximately twice that of a streptavidin tetramer. For example, the measured mass of species iv could, in principle, be consistent with a complex containing one kinesin dimer and three streptavidin tetramers (~271 kDa). However, this possibility is unlikely given that the complex was observed in solutions with excess kinesin (Fig. 2b). In addition to complex species iii-v, we also detected substantially larger species that we refer to as "higher-order complexes" (Fig. S4, ESI†). These higher-order complexes likely comprise a mixture of different species: the mass at ~500 kDa is consistent with a report of four kinesin dimers per streptavidin tetramer[8], and the mass at ~950 kDa is consistent with a report of up to 8 kinesin dimers per complex[2].

We found that the isolated kinesin protein is largely absent in mixtures at lower molar mixing ratios (for example, K:S 0.4:1, Fig. 2a). This finding indicates that all kinesin bound streptavidin during the 30 min incubation. Similarly, the isolated streptavidin protein is absent in mixtures at higher mixing ratios (for example, K:S 3.6:1, Fig. 2a), indicating that all streptavidin bound kinesin.

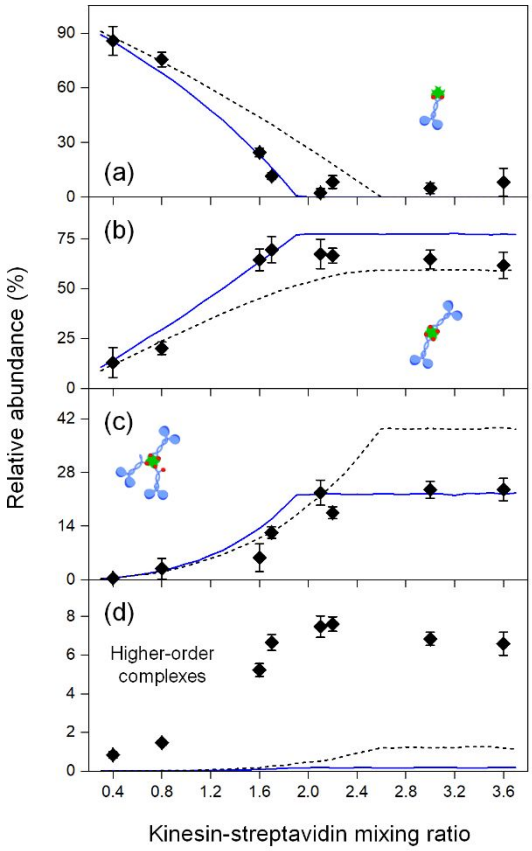

Fig. 4 Relative abundance of different complex species as a function of the kinesin-streptavidin mixing ratio. The concentration of streptavidin in each mixture was kept constant at 0.6 μM. Calculations of relative abundance excluded the isolated proteins. (a-c) Complexes with 1:1, 2:1, and 3:1 stoichiometry. Relative abundances were determined via best-fits of mass distributions to a bi-Gaussian mixture model; error bars indicate the associated fitting uncertainties. Black dashed lines indicate the predictions of a simple binding model without any fitting parameters, using the experimentally estimated kinesin-biotinylation efficiency (77%) and kinesin-streptavidin mixing ratios (as indicated). Blue solid lines indicate the predictions of the same binding model, using the best-fitted values of the kinesin-biotinylation efficiency (88%) and an overall scaling factor for the mixing ratios (1.19); only complexes with well-defined stoichiometries (panels a-c) were included in the fit. (d) Higher-order complexes. Relative abundances were estimated as the cumulative counts of masses ≥450 kDa; error bars indicate the associated counting noise. Black dashed lines (and blue solid lines) indicate the binding model predictions using the measured (and the best-fit) values of kinesin-biotinylation efficiency and kinesin-streptavidin mixing ratio as described in (a-c). Note the changes in the y-axis range in panels (a)–(d).

For most incubation ratios tested, we detected mainly isolated proteins rather than kinesin-streptavidin complexes (Fig. 2a). This observation reflects an important caveat in using mass photometry for molecular counting and abundance measurements. Briefly, mass photometry employs a differential detection method that is sensitive to proteins binding to, and unbinding from, the sample surface[20-24]. Accurate molecular counting is predicated on proteins irreversibly bound to the surface, such that the binding is counted once and only once. If the protein unbinds, the unbinding leads to a change in

interference intensity that is equal in magnitude but opposite in sign as a binding event, resulting in an apparent negative mass reading. Moreover, the unbound protein can be counted multiple times, through repeated rebinding and unbinding events, artifactually increasing the molecular counts[25]. In our experiments, we detected substantial negative mass counts for the isolated proteins (i-ii, Fig. S5, ESI†), but not kinesin-streptavidin complexes (iii-v, Fig. S5, ESI†). Factors including hydrophobicity and surface charge distribution could contribute to the unbinding rates of isolated proteins from the sample surface[25]. We speculate that the kinesin-streptavidin complexes have substantially lower unbinding rates than the isolated proteins due to simultaneous binding of both kinesin and streptavidin constituents: unbinding of the complex requires simultaneous unbinding of both constituents. This interpretation is generally consistent with increased avidity due to additional binding interactions[31] and specifically consistent with the stable binding of kinesin-streptavidin complexes over the experimental measurement time (~1 min). We therefore excluded the isolated proteins from calculations of relative abundance of complex species in the next section.

Focusing on the region of complex species (Fig. 2b), we observed more than one complex species in most kinesin-streptavidin solutions (bottom five panels, Fig. 2b). We determined the abundance of each complex species via best-fits to a bi-Gaussian mixture model (for example, Fig. S6a, ESI†). For complex species without a pronounced peak profile, we employed our measurements of molecular masses in Fig. 3 to constrain their peak positions in the fit. Additionally, for higher order complexes (Fig. S4, ESI†), we estimated their abundance as the cumulative counts of masses ≥450 kDa. Based on these abundance calculations, and excluding the isolated proteins, we determined the relative abundance of different kinesin-streptavidin complexes as a function of mixing ratio (Fig. 4). The resulting relative-abundance calculations agreed well between experiments using different preparations of the same kinesin-streptavidin mixture (Fig. S6, ESI†).

At lower mixing ratios, we found that the most abundant complex consisted of one kinesin dimer and one streptavidin (Fig. 4a), which is functionally equivalent to a single kinesin dimer and cannot drive pair-wise sliding of filaments in active matter. As the mixing ratio increased, the relative abundance of complexes with two or more kinesins increased (Fig. 4b-d). These larger complex species are appropriate for driving active matter dynamics. Supporting our hypothesis, the relative abundance of complexes with three or more kinesin dimers increased as the kinesin-streptavidin mixing ratio increased (Fig. 4c-d).

We found that changes in the relative abundance of complex species largely plateaued at a mixing ratio of ~2 kinesin dimers per streptavidin tetramer (Fig. 4). Above this mixing ratio, the relative abundance of complex species varied somewhat, but these variations were within measurement uncertainties (Fig. 4a-c) or did not exceed ~2% of the overall complex population (Fig. 4d). These observations suggest a more limited range of mixing ratios would impact active-matter length scale than previously found by Henkin et al.[4] (up to ~3.4 kinesin dimers per streptavidin tetramer).

Because each streptavidin tetramer contained only four binding sites, plateaus in the relative abundances of complex species is expected. If each kinesin dimer carried two biotin tags (100% biotinylation), we would expect a homogeneous population of complexes with 2:1 stoichiometry at the plateau. In contrast, we observed a heterogenous population of complexes containing two or more kinesins (Fig. 4b-d). Moreover, the substantial presence of three-kinesin complex (Fig. 4c) indicates that some kinesin dimers bound the streptavidin protein via a single biotin.

Employing liquid chromatography-mass spectrometry, we estimated that ~77% of kinesin monomers in the current study were biotinylated (Fig. S7b, ESI†). Note that, here we employed a standard, biotin carboxyl carrier protein-based approach to attach a single biotin tag on each kinesin monomer[9, 10]; the efficiency of biotinylation using this approach typically ranges between 50 and 80%[11]. To our knowledge, quantitative characterization of kinesin biotinylation has not been reported in prior active-matter studies.

We found that a simple binding model taking account of the kinesin-biotinylation efficiency, and kinesin-streptavidin mixing ratio, captures the main features of the observed complex distributions (Fig. 4). In this binding model, we assumed complete and stable kinesin-streptavidin binding. We assumed that the two biotins on the same kinesin dimer are coupled: once one biotin bound the streptavidin, the second biotin would also bind, provided that there was an open site on the streptavidin. We assumed that a kinesin dimer with two biotins was twice as likely to encounter a streptavidin molecule than a single biotin. We used the molar ratio of biotins and streptavidin monomers in the mixture to estimate the probability that a biotin on a kinesin dimer binds a streptavidin at each encounter. We assumed no steric hinderance between multiple kinesin dimers binding to the same streptavidin tetramer. We considered complexes with well-defined stoichiometries (containing up to four kinesin dimers). We did not consider higher-order complexes.

Using the experimentally estimated kinesin-biotinylation efficiency and kinesin-streptavidin mixing ratios, the model recovered the heterogeneous nature of the complex population, captured the initial changes in the complex heterogeneity as the mixing ratio increased, and closely approximated the relative abundance of two-kinesin complexes in the plateau (black dashed lines, Fig. 4). The predicted presence of three-kinesin complex and higher-order complexes, however, deviated from experiments in their respective plateau values (Fig. 4c-d). These deviations could reflect aggregation into high-order complexes that was not considered in the model. There may also be steric hinderance between multiple kinesins binding to the same streptavidin, which would decrease the relative abundance of the three-kinesin complexes and increase the relative abundance of the smaller complexes. Another deviation from experiments is that the model predicted that the complex heterogeneity plateaued at a mixing ratio ~30% higher than that estimated in experiments (Fig. 4).

This deviation may reflect uncertainties in quantitative determination of the molar mixing ratio in microvolume samples.

To account for measurement uncertainties inherent in the determination of protein mixing ratios and biotinylation efficiency, we varied the efficiency of kinesin biotinylation, and an overall scaling of the mixing ratio, in our model. The resulting best-fit model provided closer approximations to experiments (blue solid lines, Fig. 4), with best-fitted parameters that were within ~20% of their experimental values (Fig. S8, ESI†). Note that, higher-order complexes were not included in the model or the fit, and the deviation between experiments and model predictions (Fig. 4d) may reflect some aggregation into higher-order complexes.

A simplification in our binding model is that it considers the kinesin-streptavidin mixing ratio, rather than the concentrations of each protein. This simplification is supported by the overall agreement between model predictions and experiments in Fig. 4. We also performed additional experiments in which we kept the mixing ratio constant while we varied the concentrations of kinesin and streptavidin proteins over an 8-fold range (Fig. S9, ESI†). We found that, although the relative abundance of complex species varied somewhat with protein concentration, our model is appropriate for the protein concentrations employed in the current study (Fig. S9, ESI†), which were chosen based on concentrations commonly used in active matter experiments[1, 6, 7].

Because it is non-trivial to quantitatively control biotinylation efficiency in protein expression, we employed our simple model to explore in more detail how kinesin-biotinylation efficiency impacts the heterogenous distribution of kinesin-streptavidin complexes (Fig. S10, ESI†). In the limit that each kinesin dimer carries two biotin tags (100% biotinylation efficiency), the model recovers the anticipated homogeneous population of complexes with 2:1 stoichiometry when biotin is in excess (dashed lines, Fig. S10, ESI†). Incomplete kinesin biotinylation gives rises to larger complexes with 3:1 or 4:1 stoichiometry (solid lines, Fig. S10c-d, ESI†). These larger complexes have the potential to increase the number of kinesins simultaneously bound to microtubules, which empirically decreases the macroscopic length scale of the resulting microtubule-based active matter[4]. For a given biotinylation efficiency below 100%, our model predicts that the relative abundance of these larger complexes increased as a function of mixing ratio, before plateauing when biotin is in excess (Fig. S10c-d, ESI†). This prediction is consistent with experiments in the current study (Fig. 4), supporting our hypothesis and providing intuition on how the characteristic length scale of the active matter can decrease as the mixing ratio increases (such as that previously reported in Henkin et al.[4]). As the efficiency of kinesin biotinylation decreased, the relative abundance of the larger complexes (3:1 or 4:1 stoichiometry) plateaued at higher values, and the mixing ratio at which the plateau was reached also increased (Fig. S10c-d, ESI†). These predictions further highlight kinesin-streptavidin biotinylation as a key factor in determining the kinesin-streptavidin complex distribution, providing a possible explanation for the impact of mixing ratio on the characteristic length scale observed in active matter experiments[4].

Conclusions

Here we employed mass photometry to determine the stoichiometry of Kinesin-streptavidin complexes widely employed in microtubule-based active matter studies. We found that, contrary to the assumption of a 2:1 complex stoichiometry, populations of kinesin-streptavidin complexes are heterogenous (Figs. 2-4), and that the heterogeneity depends on the kinesin-streptavidin mixing ratio (Figs. 2 and 4). We captured the key features of the measured distributions using a simple binding model (Fig. 4). Our model indicates that the efficiency of kinesin-biotinylation is an unexplored determinant of kinesin-streptavidin complex distribution (Fig. S10, ESI†).

It has long been established that that the kinesin: streptavidin mixing ratio can impact the key characteristics of active matter[1, 4]. Here we found that the relative abundance of complexes containing three or more kinesin dimers depended sensitively on the kinesin-streptavidin mixing ratio (Fig. 4). Because these larger complexes can increase the number of kinesins simultaneously bound to microtubules, the observed changes in the relative abundance of these larger complexes could provide a mechanistic explanation for the effect of mixing ratio on the characteristic length scale reported previously[4]. Moreover, our model indicates that the effect of mixing ratio on complex heterogeneity is highly sensitive to the efficiency of kinesin biotinylation (Fig. S10, ESI†). Together, our study supports the hypothesis that the macroscopic length scale of the active matter system correlates negatively with the microscopic stoichiometry of the kinesin-streptavidin complexes. Future investigation may help extend our simple model to consider protein concentration, steric hinderance, and higher-order complex formation.

More generally, in addition to active-matter investigation, the biotin-streptavidin chemistry is widely used to induce complex formation in chemical and biological experiments, as well as in biosensor applications[32]. We anticipate that the mass photometry technique used in the current study may be broadly applicable for elucidating the nature of complex formation that underly these experiments and/or biosensing applications.

Author Contributions

J. X. conceived and designed the study; J. X. and N. J. S. B. performed the experiments and analyzed the data; J. X. and K. C. N. developed the binding model; Y. S. generated the recombinant motor protein; J. X. wrote the manuscript. K. C. N. and Y. S. edited it. All the authors reviewed the paper.

Conflicts of interest

There are no conflicts to declare.

Data availability

Data underlying Figs. 2-4 and Figs. S1-S10 are available at https://doi:10.5061/dryad.1rn8pk12h.

Acknowledgements

This work was supported by the National Institutes of Health (R15 GM120682 to J. X.) and the Intramural Research Program of the National Heart, Lung, and Blood Institute, National Institutes of Health (ZIAHL001056 to K. C. N.).

We thank Di Wu, Grzegorz Piszczek, Duck-Yeon Lee, Yasuharu Takagi, and Adam Fineberg for support and comments. We thank the Biophysics Core Facility and the Biochemistry Core Facility at the National Heart, Lung, and Blood Institute, National Institutes of Health, for the use of the OneMP instrument and for providing mass spectroscopy measurements. We thank Zvonimir Dogic, Shibani Dalal, the Brandeis Biomaterials Facility, and the National Science Foundation grant no. DMR 2011846 for providing the K401-BIO-6H plasmid. We thank Esme P. Neuman for illustrations of kinesin dimer. We thank the reviewers for insightful comments and suggestions.

References

1 F. J. Nedelec, T. Surrey, A. C. Maggs and S. Leibler, *Nature*, 1997, **389**, 305-308.
2 T. Surrey, F. Nedelec, S. Leibler and E. Karsenti, *Science*, 2001, **292**, 1167-1171.
3 T. Sanchez, D. T. Chen, S. J. DeCamp, M. Heymann and Z. Dogic, *Nature*, 2012, **491**, 431-434.
4 G. Henkin, S. J. DeCamp, D. T. Chen, T. Sanchez and Z. Dogic, *Philos. Trans. A Math Phys. Eng. Sci.*, 2014, **372**, 20140142.
5 P. Chandrakar, J. Berezney, B. Lemma, B. Hishamunda, A. Berry, K. T. Wu, R. Subramanian, J. Chung, D. Needleman, J. Gelles and Z. Dogic, *Soft Matter*, 2022, **18**, 1825-1835.
6 T. E. Bate, M. E. Varney, E. H. Taylor, J. H. Dickie, C. C. Chueh, M. M. Norton and K. T. Wu, *Nat. Commun.*, 2022, **13**, 6573.
7 A. M. Tayar, L. M. Lemma and Z. Dogic, *Methods Mol. Biol.*, 2022, **2430**, 151-183.
8 B. Najma, W. S. Wei, A. Baskaran, P. J. Foster and G. Duclos, *Proc. Natl. Acad. Sci. U. S. A.*, 2024, **121**, e2300174121.
9 E. Berliner, H. K. Mahtani, S. Karki, L. F. Chu, J. E. Cronan, Jr. and J. Gelles, *J. Biol. Chem.*, 1994, **269**, 8610-8615.
10 R. Subramanian and J. Gelles, *J. Gen. Physiol.*, 2007, **130**, 445-455.
11 B. K. Kay, S. Thai and V. V. Volgina, *Methods Mol. Biol.*, 2009, **498**, 185-196.
12 J. Xu, Z. Shu, S. J. King and S. P. Gross, *Traffic*, 2012, **13**, 1198-1205.
13 P. Chandrakar, M. Varghese, S. A. Aghvami, A. Baskaran, Z. Dogic and G. Duclos, *Phys. Rev. Lett.*, 2020, **125**, 257801.
14 L. Giomi, *Physical Review X*, 2015, **5**, 031003.
15 L. M. Lemma, S. J. DeCamp, Z. You, L. Giomi and Z. Dogic, *Soft Matter*, 2019, **15**, 3264-3272.
16 S. Beretta, L. Lunelli, G. Chirico and G. Baldini, *Appl. Opt.*, 1996, **35**, 3763-3770.
17 J. Stetefeld, S. A. McKenna and T. R. Patel, *Biophys. Rev.*, 2016, **8**, 409-427.
18 I. Wittig, H. P. Braun and H. Schagger, *Nat. Protoc.*, 2006, **1**, 418-428.
19 H. Zhang and P. Guo, *Methods*, 2014, **67**, 169-176.
20 G. Young, N. Hundt, D. Cole, A. Fineberg, J. Andrecka, A. Tyler, A. Olerinyova, A. Ansari, E. G. Marklund, M. P. Collier, S. A. Chandler, O. Tkachenko, J. Allen, M. Crispin, N. Billington, Y. Takagi, J. R. Sellers, C. Eichmann, P. Selenko, L. Frey, R. Riek, M. R. Galpin, W. B. Struwe, J. L. P. Benesch and P. Kukura, *Science*, 2018, **360**, 423-427.
21 P. Kukura, H. Ewers, C. Muller, A. Renn, A. Helenius and V. Sandoghdar, *Nat. Methods*, 2009, **6**, 923-927.
22 J. Ortega-Arroyo and P. Kukura, *Phys. Chem. Chem. Phys.*, 2012, **14**, 15625-15636.
23 M. Liebel, J. T. Hugall and N. F. van Hulst, *Nano Lett.*, 2017, **17**, 1277-1281.
24 D. Cole, G. Young, A. Weigel, A. Sebesta and P. Kukura, *ACS Photonics*, 2017, **4**, 211-216.
25 Refeyn Ltd, *OneMP (version 1.3) User Manual*.
26 D. E. Hyre, I. Le Trong, E. A. Merritt, J. F. Eccleston, N. M. Green, R. E. Stenkamp and P. S. Stayton, *Protein Sci.*, 2006, **15**, 459-467.
27 M. Srisa-Art, E. C. Dyson, A. J. deMello and J. B. Edel, *Anal. Chem.*, 2008, **80**, 7063-7067.
28 A. Chilkoti and P. S. Stayton, *J. Am. Chem. Soc.*, 1995, **117**, 10622-10628.
29 L. Deng, E. N. Kitova and J. S. Klassen, *J. Am. Soc. Mass Spectrom.*, 2013, **24**, 49-56.
30 D. Wu and G. Piszczek, *Anal. Biochem.*, 2020, **592**, 113575.
31 A. V. Terskikh, J. M. Le Doussal, R. Crameri, I. Fisch, J. P. Mach and A. V. Kajava, *Proc. Natl. Acad. Sci. U. S. A.*, 1997, **94**, 1663-1668.
32 C. M. Dundas, D. Demonte and S. Park, *Appl. Microbiol. Biotechnol.*, 2013, **97**, 9343-9353.